From Multi-Sensor Tracking of Sea Surface Films to Mesoscale and Sub-Mesoscale Sea Surface Current Fields

Benjamin Seppke[*a], Martin Gade[b], Leonie Dreschler-Fischer[a]
[a] University of Hamburg, Dept. of Informatics, Vogt-Kölln-Str. 30, 22527 Hamburg, Germany;
[b] University of Hamburg, Inst. of Oceanography, Bundesstr. 53, 20146 Hamburg, Germany

ABSTRACT

The knowledge about mesoscale and sub-mesoscale sea surface current fields is of high interdisciplinary interest, since it results in a better understanding of ocean-atmosphere interactions. However, many available numerical model results are of resolutions, which are too coarse to investigate mesoscale and sub-mesoscale turbulent features like eddies, particularly in coastal waters. In this work we present the results of tracking biogenic and anthropogenic surface film signatures on multi-sensor satellite images (SAR and multispectral images) to estimate the local sea surface current field. The main advantage of this approach is that the resolution of the derived current fields depends mainly on the resolution of the images, which have been used for tracking. Due to the large temporal distance between two acquisitions of a scene and the high variability of the tracked sea surface films, classical tracking methods, e.g. feature based or Optical Flow methods may not be applicable to successfully track the imaged signatures of the surface films. In this work, we use our former developed generic framework, which ensures the applicability and increases the stability of the results for well-known tracking and Optical Flow algorithms. With this framework, it is e.g. possible to compute the sea surface current field using Optical Flow approaches even for large spatiotemporal distances and with partial scene coverage. We present and compare the results of different tracking algorithms by means of tracking biogenic sea surface films. The investigated areas are the Baltic Sea and the Black Sea. We present the use of Landsat TM, SeaWiFS, ERS-2, TerraSAR-X and RADARSAT-2 data for the derivation of sea surface currents. The resolution of the images used varies from moderate to fine resolution, which allows the derivation sea surface current fields of moderate to fine resolutions.

Keywords: surface currents, multi-spectral, SAR, surface films, tracking, Optical Flow, pattern matching

1. INTRODUCTION

The knowledge about mesoscale and sub-mesoscale sea surface current fields is of high interdisciplinary interest, since it results in a better understanding of ocean-atmosphere interactions. However, many available numerical model results are of resolutions, which are too coarse to investigate mesoscale and sub-mesoscale turbulent features like eddies, particularly in coastal waters. In [1] we have already shown that remote sensing images from satellite-borne sensors working at the same or different electromagnetic frequencies can be used to derive ocean current fields, if the same features are visible in the different data sets and if the data were acquired quasi-simultaneously. In contrast to other studies, which have been performed on the use of single sensor types (i.e. either optical or radar), we propose the combined use of different sensors for the estimation of the sea surface current. Since the traceable objects (tracers) must then be visible on all used sensor images, we have chosen marine surface films as tracers. They are well suited for this task, because they can change both the sea surface roughness [2] and its emissivity of electromagnetic waves [3] and may thus be visible on both, radar and optical imagery.

In this work, we will give a summary of the recent research in the field of current estimation by means of tracking sea surface films in multimodal image sequences. Beginning with the some examples for the derivation of mesoscale sea surface current fields in the Northern Baltic Sea, we put our emphasis on the derivation of sub-mesoscale sea surface current fields, for which we will use high-resolution synthetic aperture radar (SAR) images, acquired namely by the RADARSAT-2 and TerraSAR-X satellite platforms.

[*] seppke@informatik.uni-hamburg.de; phone: +49 40 42883-2171; fax +49 40 42883-2572

The high-resolution SAR satellite data, which we use for tracking of signatures of sea surface films, is provided by means of the DTeddie project. The name DTeddie stands for "Detection and Tracking of Small Scale Eddies Using High-Resolution RADARSAT-2 and TerraSAR-X Imagery" and is supported by the Canadian Space Agency (CSA) and the German Space Agency (DLR). The project consists of an international collaboration between the University of Hamburg (Dept. of Informatics and Institute of Oceanography) and the remote sensing research group at the IKI (Russian Space Research Institute, Moscow). In this work we focus on the algorithmic (tracking) part, which is developed at the University of Hamburg, and the results we achieved so far.

While satellite images of moderate resolution may be sufficient for the derivation of mesoscale sea surface current fields, only the high resolution provided by RADARSAT-2 and TerraSAR-X data allows to study small scale eddies with sizes of less than 1 km in the area of the Black Sea. With characteristic sizes less than the Rossby deformation radius (about 18 km for the Black Sea) these vortical structures cannot be imaged by optical or IR sensors due to the absence of thermal and optical contrasts as well as due to limited spatial resolution. The development of the corresponding tracking algorithms is insofar challenging as nearly all existing algorithms have their origin in the research area of computer vision or more precisely: video analysis.

If we switch from this are to the use of satellite imagery for tracking, some major differences become evident [4]:

1. Different sensors are used for the acquisition.
2. There are non-equidistant and potentially large time gaps between each acquisition.
3. The spatial distance between the tracers is usually much higher between each image of the series.
4. The geometric size of the images is larger and not uniform.
5. Some image sources (e.g. SAR) require an advanced preprocessing before the tracking process.

Especially the challenges 2 and 3 become even more challenging for the derivation of sub-mesoscale sea surface current fields, since these images need to have higher resolutions. This yields to larger absolute (pixel) distances between the tracers in subsequent images compared to the moderate resolution images. To cope the challenges at the mesoscale we will present a framework, which supports the decomposition of large motion into a global motion model and small motion deviations from that model, and introduce a feature-based fast normalized cross-correlation technique into the field of sea surface film tracking [5].

We also adapted differential methods, like e.g. the approach of Horn and Schunck [6] into the framework and achieved promising results at the measurement of mesoscale currents.

2. REGIONS OF INTEREST

To demonstrate the derivation of mesoscale and sub-mesoscale sea surface current from different satellite sensors, we distinguish between two regions with corresponding regions of interest (ROIs). For the first region, which covers a large area of the Baltic Sea, three different satellite images of different modalities (multispectral, SAR) are available. For the second region, which covers the coastal area at Gelendzhik (Black Sea), two different high-resolution SAR images have been acquired. The dates and additional environment conditions as well as further available data will be introduced in the following subsections.

2.1 First region: Northern Baltic Sea

The first area is the Northern Baltic Proper, north of the Swedish island of Gotland. On July 15, 1997, a day with extensive cyanobacterial blooms in the northern Baltic Proper, data from three different satellite sensors were acquired over the same area, including the Thematic Mapper (TM) aboard Landsat, the Synthetic Aperture Radar (SAR) aboard ERS-2 and the Wide-Field Scanner (WiFS) aboard IRS-1C. In fig. 1 a map of the first region and the corresponding ROI is shown. Here, the satellite coverage is highlighted for each sensor.

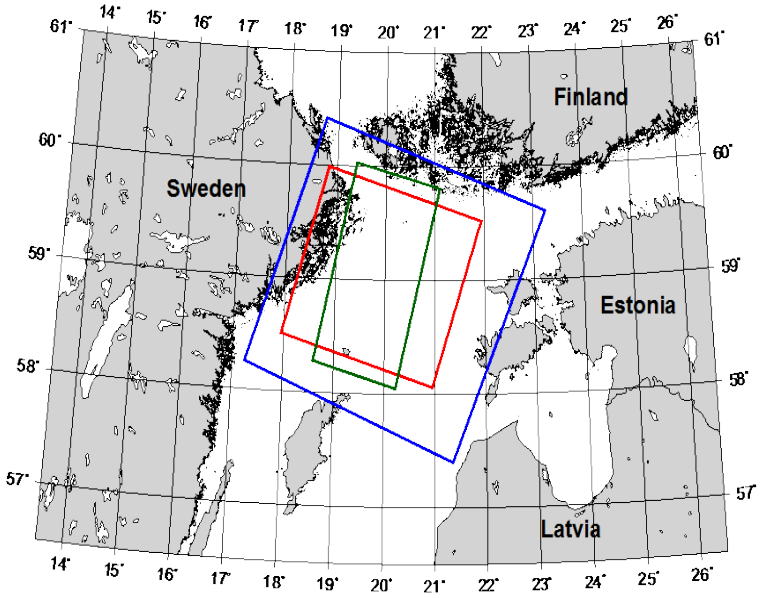

Figure 1. Map of the Northern Baltic Sea (Baltic Proper) indicating the location of the satellite images used for the first study presented herein at July 15, 1997: ERS-2 SAR (green), Landsat TM (red) and IRS WiFS (dark blue). Image source: [7].

The high morpo-dynamic of the biogenic surface films requires a small time gap between the acquisitions. At the first region, the three satellite sensors image the area within less than two hours, which is considered to be sufficient. Additionally all sensors provide a spatial resolution of at least 188 m per pixel, which is sufficient for the detection of mesoscale surface current features. Further satellite characteristics of each acquisition can be found in tab. 1.

Table 1. Satellite characteristics for the first region. The date of all acquisitions is July 15, 1997.

Platform	Sensor	Resolution (m)	Time (UTC)
Landsat 5	TM	30.0	08:57
ERS-2	SAR	12.5	09:47
IRS-1C	WiFS	188.0	10:26

Due to an extensive algae bloom, signatures of accumulated algae are visible on all of the acquisitions, e.g. as brighter linear structures in most parts of the (multispectral) Landsat TM image (fig. 2). For further analysis we have selected a central ROI, which has been imaged by all three sensors. This region is shown in fig. 2 superimposed on a false-color representation of the Landsat TM image. Fig. 2 also shows a lot of vortical structures of surface films, which may correspond to local sea surface current turbulences.

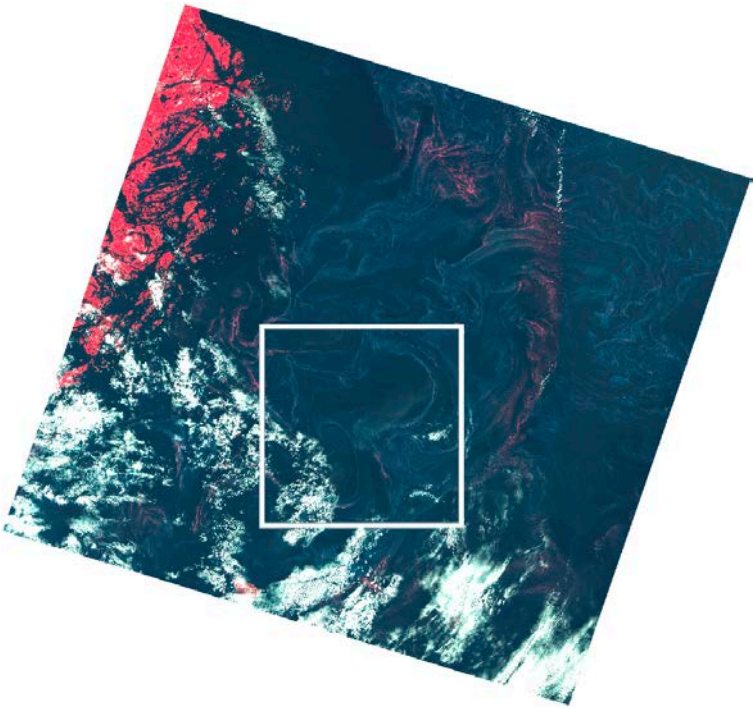

Figure 2. False color representation of the Landsat TM image acquired at July 15, 1997: The white square denotes the first region of interest. Brighter linear signatures refer to sea surface films and white signatures denote clouds.

Additional information on this scene comprise that during the acquisitions there has been a wind of about 3 m/s coming from northwest and an inflow of colder water masses from the north [1]. For this ROI, we also have access to the results of numerical current models provided by the German Federal Maritime and Hydrographic Agency (BSH). These results will be presented and used for evaluation in the discussion, since there are no in-situ measurements available.

2.2 Second region: Gelendzhik (Black Sea)

The second region is the area around Gelendzhik (Black Sea). Here we are presenting the use of high-resolution SAR images to derive sub-mesoscale sea surface current fields. The images used in this study have been acquired by means of the DTeddie project, in which access to TerraSAR-X and RADARSAT-2 images is granted. Due to legal requirements, we are only allowed to acquire RADARSAT-2 images over Russian territory, where vortical structures of surface films have been detected during past research [8]. A map of the region is shown in fig. 3.

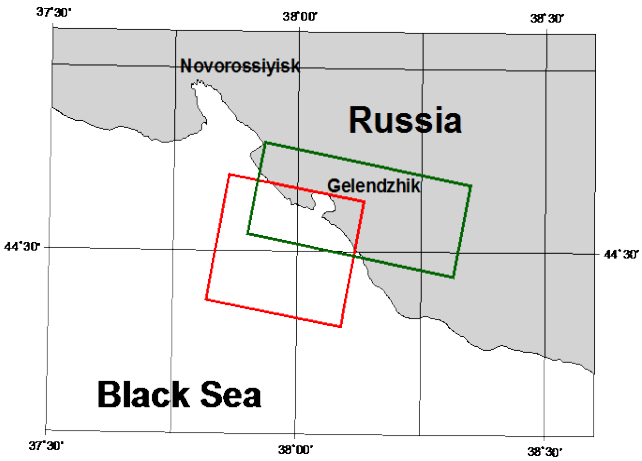

Figure 3. Map of the Black Sea coastal area of Gelendzhik indicating the location of the satellite images used for the second study presented herein at October 11, 2011: RADARSAT-2 (green) and TerraSAR-X (red).

The images, which we use to derive the sub-mesoscale sea surface current, have been acquired on October 11, 2011. Both SAR sensors imaged the area within a time gap of less than 10 minutes. Due to the short time lag, only very small changes in the images occur and become visible. Both image resolutions are about 3 m per pixel (tab. 2). This resolution is fine enough to derive sub-mesoscale features of the surface currents as well as features of a much finer scale. Regarding the quality of both images, the RADARSAT-2 image suffers from more speckle noise compared to the TerraSAR-X image. The origin of this higher amount of speckle noise the Ultra-Fine mode of RADARSAT-2, which creates images based on only one look. The TerraSAR-X image on the other hand, was computed by the corresponding agency using an equivalent number of looks of 1.3.

Table 2. Satellite characteristics for the second region. The date of all acquisitions is October 11, 2011.

Platform	Sensor	Resolution (m)	Time (UTC)
RADARSAT-2	C-Band ASAR	2.8	03:37
TerraSAR-X	X-Band ASAR	3.0	03:44

Due to an accumulation of surface films during the image acquisitions, the sea surface waves of small wavelengths are also damped in high-resolution SAR imagery. These accumulations can thus be seen as darker linear structures on both SAR images. These structured are highlighted in fig. 4. Unlike the first ROI, there are no vortical structures present, which may hint to local sea surface turbulences. During field excursions performed by our Russian project partners, which have been carried out co-located with the satellite overflows, in-situ current measurement using an Advanced Doppler Current Profiler (ADCP) are available. These measurements will be used for evaluation purpose in the discussion. Numerical current model data have not been available for this region.

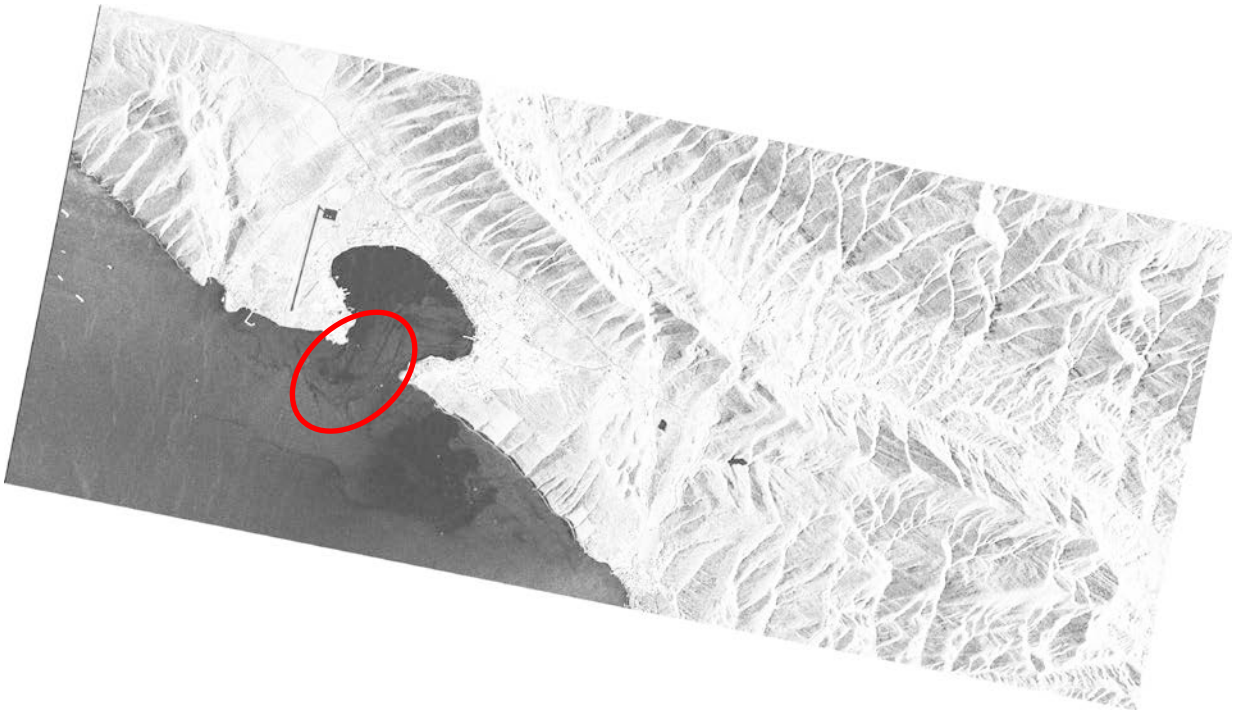

Figure 4: The orthorectified TerraSAR-X image showing the bay of Gelendzhik and the coastal area as well as the Black Sea. The brightness has been raised in order to ensure the visibility of the biogenic marine surface films' signatures near the bay area (marked red).

3. METHODS

Since the research field of motion detection from image sequences is nearly as old as the field of computer vision or image processing, a lot of algorithms have been developed. Starting in the 1980s with [6] and [9], even nowadays, new algorithms are being constructed, most often tailored to specific needs or special application contexts. In contrast to this development, our claim is not to develop a new adapted algorithm, but provide a framework, which makes the well-known and theoretically proven algorithms applicable to the application domain of deriving sea surface currents by tracking sea surfaces film at satellite images of different sensors and sensor modalities. We therefore distinguish between two categories of algorithms:

1. Feature-based approaches
2. Gradient-based approaches

The feature-based approaches follow the idea, that features can be extracted for each tracer on each image. The displacement of a feature from image to image can then be computed using a statistical comparison operator, like e.g. a correlation value. Based on the estimated similarities a matching of the features can yield to a map of displacements – the sea surface current fields. If we assume that its surrounding image patch can characterize each feature, a famous maximum likelihood estimator is the maximum cross-correlation (MCC) approach. Emery et al. used this basic matching approach to derive large sea surface currents from infrared satellite imagery [10]. This approach has, however, one major disadvantage: It may neither be applicable for images of different sensors nor different sensor modalities. To cope this, one could use a normalized cross correlation combined with a maximum likelihood estimator. But this procedure has another drawback: It may be very slow for large displacements and a large amount of features to track. Thus, in [1] we propose the use of two techniques to enhance the normalized feature-based matching:

1. Based on both images, estimate the global displacement of the overall movement. This is done by an adapted version of the algorithm described by Sun in [11].
2. Use a fast variant of the normalized cross correlation, to compute only the remaining local part of the tracers' motion. The fast normalized cross-correlation was described in [5]. It is based on the Fast Fourier Transform [12] and uses sum-tables for caching.

By means of the developed framework, the second point is exchangeable with e.g. a shape-based comparison operator or the classical (un-normalized) cross-correlation for comparison purpose. Additionally, relaxation techniques have been developed to favor smooth matching strategies instead of the local maximum likelihood of the assignment (see [7]).

Another class of approaches is based on the Optical Flow Constraint Equation (OFCE), which relates the changes in image brightness to the displacement / motion of the objects:

$$\frac{dIS}{dt} = 0 \quad \Leftrightarrow \quad \frac{\partial IS}{\partial x}u + \frac{\partial IS}{\partial y}v + \frac{\partial IS}{\partial t} = 0, \tag{1}$$

where $IS(x,y,t)$ is the image sequence function, u and v the displacement functions in x- and y-direction respectively.

This method is applicable if and only if the values of image brightness are comparable. It is, due to the algorithmic base, not applicable to sensors of different modalities, like e.g. multispectral combined with SAR images. Even if the images haven been acquired by comparable sensors, there are two aspects in the application context of this work, which may forbid an application. Firstly, there shall be no (moving) coverage of scene items. But, in multispectral satellite images, clouds may cover different image parts in image sequences and thus yield to wrong results. Another challenging aspect is the occurrence of large displacements between two consecutive images. If the motion is two high (usually more the a few pixel), the dependency between the spatio-temporal gradient vanishes in eq. 1. As a result wrong displacement vectors will be derived.

To cope the issue of large displacements, we again use the global motion estimation, which was introduced earlier for the feature-based approaches. Since it works separately from the motion estimation algorithms, we propose the use of this extension for the gradient-based approaches as well. If this is still not sufficient, image pyramid strategies can be used to restore the coherence between the spatio-temporal gradient and the estimated motion.

The naïve solution to the partial occlusion of the sea surface by clouds would consist of a mask (e.g. pixels covered by clouds or belonging to land) and the exclusion of these pixels from image processing. This solution, however, results in errors that are propagated from the boundary of the mask, since the gradient-based approaches use averaging and propagation among larger image regions of the image series. To solve this problem, all gradient-based algorithms have been redefined using only pure local or convolution operations. The smoothing is then performed by a convolution of the image with a Gaussian, the gradient by a convolution with derived Gaussians etc. The advantage of this approach is that all sources of error are now caused by the convolution of masked and non-masked areas. Instead of adapting each algorithm, we can generically replace the basic discrete convolution by the so-called normalized convolution [13]:

$$K *_M I = \frac{K * I}{K * M}, \tag{2}$$

where K is the convolution kernel, $I(x,y)$ is an image function and M with $dom(I) = dom(M)$ is the mask.

The use of the normalized convolution defines a theoretically proven base for the optical flow algorithms with respect to the correct processing of partially covered image areas. The user still has to provide such an image mask, e.g. based on the multispectral images, which shall be used to derive the sea surface currents. For SAR images, such a masking procedure is not needed for clouds, since microwave penetrate though clouds without interference. With these adaptions, the gradient-based approaches become applicable in the domain of this work for the first time [7].

4. DISCUSSION

To further distinguish between the two regions, we separate the presentation and discussion of the results into two subsections. The first covers the mesoscale sea surface current derivation using the data of the first ROI, whereas in the second subsection the sub-mesoscale derivation will be described using data of the second ROI.

4.1 Mesoscale sea surface currents derived for the first ROI

Three different satellites imaged the first ROI on July 15. 1997. Two of three sensors, namely the Landsat TM and the IRS WiFS, are working in the same modality: multispectral images and at comparable spectral bands. Thus these images can be used to either gradient- or feature-based derivation of the sea surface currents. On the other hand, the SAR image, which has been acquired in between the two multispectral images, forces us to use normalized feature matching for current derivation. While in [7] many different algorithms and parameter settings have been investigated, in this study we only present the best configurations with respect to the numeric model current fields. The matching results of the fast normalized cross-correlation ore shown for both successive image pairs in fig. 5.

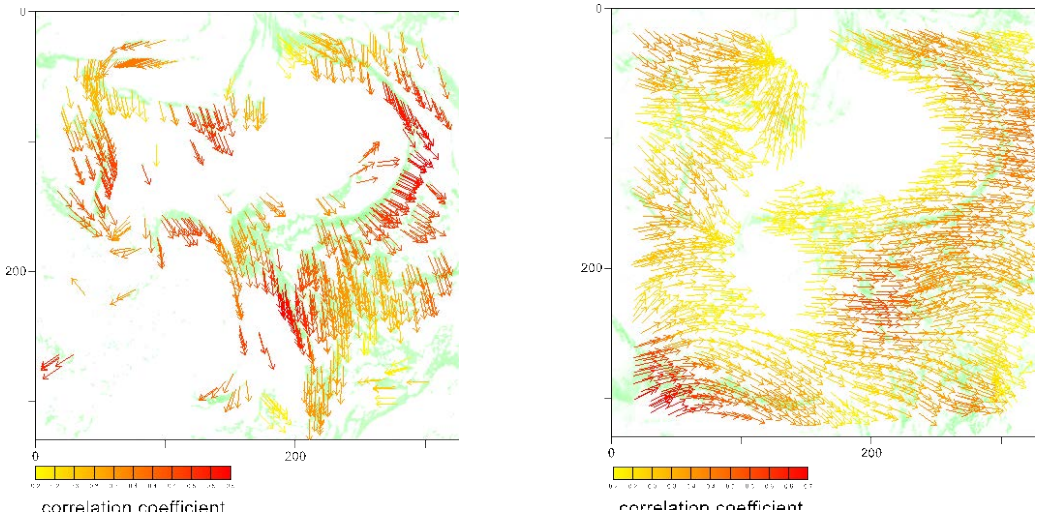

Figure 5: The results of the first ROI. Left: TM → SAR, right: SAR → WiFS. Features have been detected as local intensity maxima within areas, which have been classified as surface films. The mask size for the cross-correlation is 31x31 pixel, the maximal distance is 15 pixel. Instead of the maximum likelihood, an iterative Gaussian smoothness assignment was performed. Image source: [7].

Fig. 6 shows the results of a feature-based and a gradient-based approach in comparison for the third image pair, where the TM and the WiFS image are being analyzed. Since the gradient-based approach results in a non-weighted result, no correlation scale is given here. Additionally, the gradient-based approach results in a very dense surface current field, since displacement vectors are derived for each pixel.

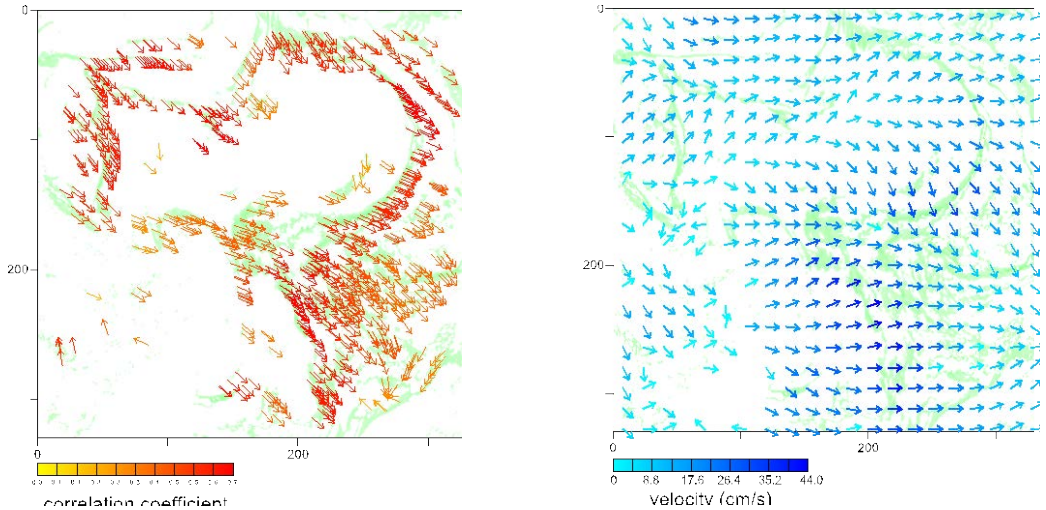

Figure 6: The results of the first ROI for TM → WiFS. Left: Features have been detected as local intensity maxima within areas, which have been classified as surface films. The mask size for the cross-correlation is 31x31 pixel, the maximal distance is 15 pixel. Instead of the maximum likelihood, an iterative Gaussian smoothness assignment was performed. Right: The result of a Gaussian gradient based Horn and Schunck approach, subsampled to 20x20 vectors. The parameters used are: α=5, σ=2. The estimation was based on image pyramids of 4 levels. Intermediate results have been propagated to the next level by Thin Plate Spline warping. Image source: [7].

The main differences between the three feature-based results are the different density of the resulting current fields. The reason is that each pair, which includes the TM image, has much fewer images to track. This is caused by the clouds, which cover large parts of this image (fig. 2). All derived current fields are quite smooth and consist of high correlation coefficients and thus can be considered qualitatively reliable. In order to establish a quantitative evaluation, we compare the derived results with the numeric model current fields. The model results are a much lower resolution compared with the derived sea surface current fields (fig. 7). Due to the sampling theorem, we have to quantitatively compare the derived results with the model results at the model scale.

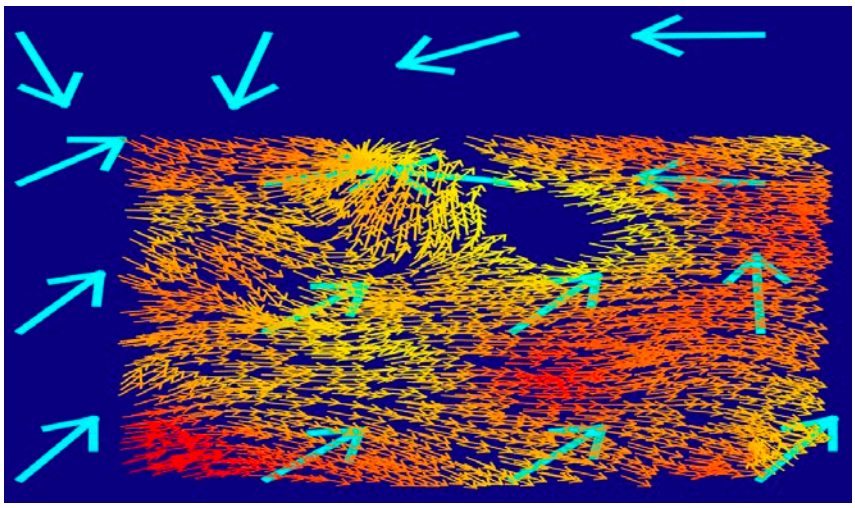

Figure 7: Comparison of the model results (bold arrows) with the feature-based derived currents from SAR → WiFS (arrows in the foreground). The model results were accumulated from 09:45 – 10:30 UTC. The model vectors are not to scale. Image source: [7]

In [7] we have studied the results of even more feature- and gradient-based approaches, which have been implemented in the developed framework. Since nearly all algorithms were able to produce comparable results, the presented results can be discussed as representatives. When compared to the numeric model results, we see a good overall agreement with the derived currents. The convergence zone, which is predicted by the model, could also be found in the derived currents but slightly differs from the predicted one. The reason for this could not finally be determined. Possible explanations may be the different data used for modeling, the deeper water mass modeling (model: 0-6 m, derived: only first cm) or the coarser resolution of the model.

4.2 Sub-mesoscale sea surface currents derived for the second ROI

Two high-resolution SAR sensors imaged the second region within 8 minutes. Due to the short acquisition interval and the expected motion of the surface films, the displacement vectors are considered to be quite small, compared with the first ROI. Although both sensors are of the same modality, it is not possible to either use un-normalized feature-based or gradient-based approaches. The reason is, that both acquisitions are performed at different radar bands and with different polarization settings, which results in different normalized radar backscatter coefficients (NRCS).

To reduce the strong speckle noise on both images, we applied a Gamma-MAP filter with a filter size of 11x11 pixel to each orthorectified and co-registered image [14]. Afterwards, a manual feature detection has been performed on the corrected RADARSAT-2 image. Fig. 8 shows the detected features of this ROI superimposed on the second (the filtered TerraSAR-X) image. Only low displacements become visible in fig. 8, since the features positions still correspond well with the darker linear signatures on the TerraSAR-X image. Mainly visible for the group of south most features, a uniform displacement in northeastern direction can be observed.

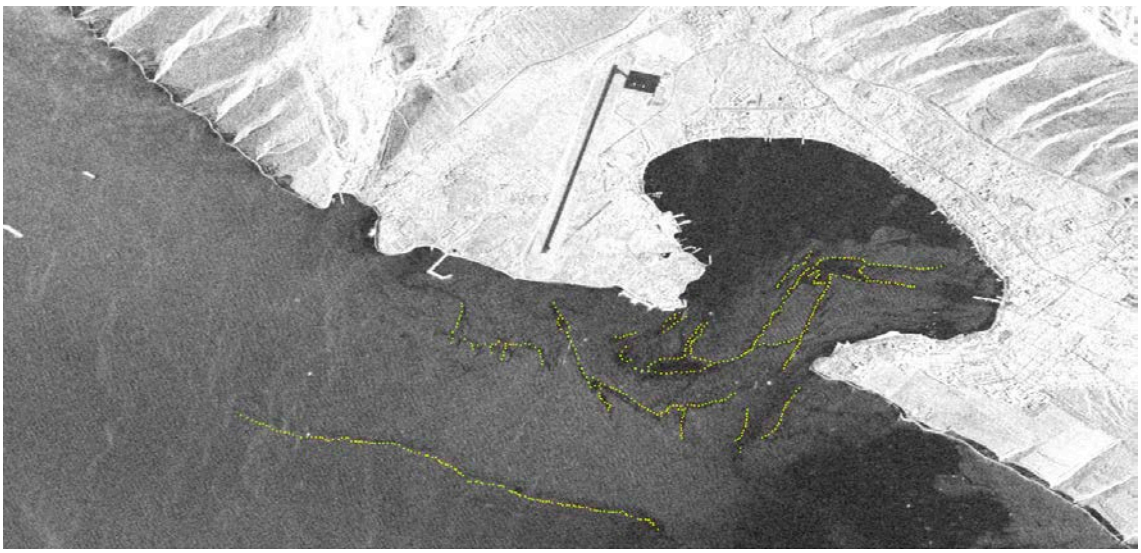

Figure 8: The Gamma-MAP filtered TerraSAR-X image. Darker linear areas of lower backscatter may correspond to biogenic surface films. Superimposed (yellow): features, which have been derived for the first image (RADARSAT-2). The image size is 18.3 x 12.2 km^2.

For the fast normalized cross-correlation, an image patch of 61x61 pixels (~ 183x183 m^2) around each feature from the RADARSAT-2 image is used as a template. Based on these feature templates, the fast normalized cross-correlation with a search radius at most 60 pixels (~ 180m) is performed. The expected maximum current velocity mainly influences the choice of the search radius. In this case, 60 pixels were chosen. This corresponds to a maximum velocity of about 40 cm/s, which shall be sufficient for this area. The most notable result of the normalized cross-correlation is that the derived displacement vectors with the highest correlation coefficient are very noisy and pointing in different directions around the features. Thus, instead of using a maximum likelihood assignment, we propose to apply the smooth assignment, which has already been used for the first ROI. To support the smooth assignment, the 10 best matches have been collected for each feature. The result of this assignment process is shown in fig. 9, where the surface current vectors are plotted onto the TerraSAR-X image. In addition, the results of the ADCP measurements are also overlaid.

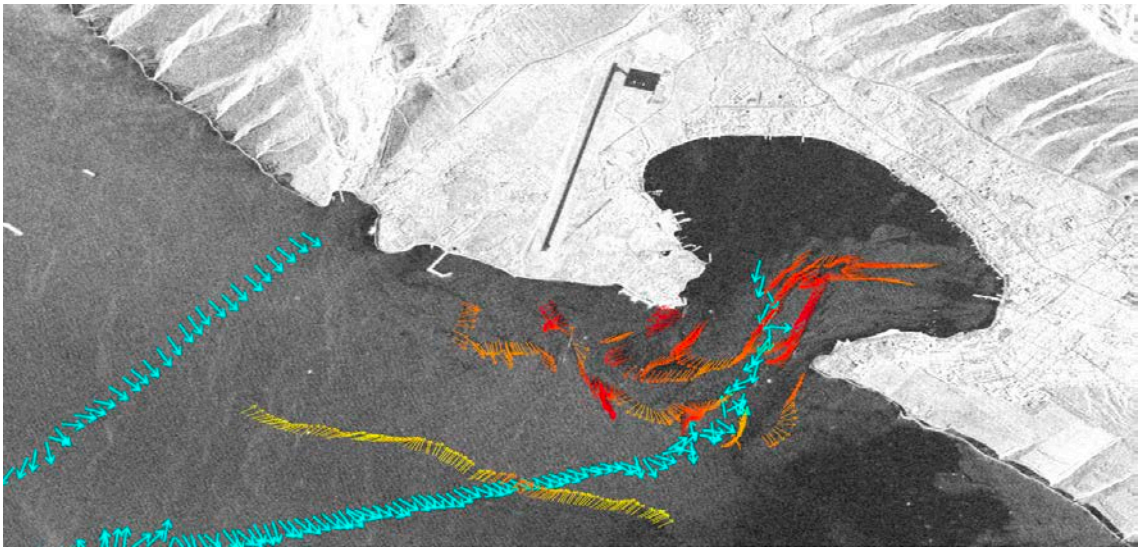

Figure 9: The results of the smooth assignment of the fast normalized cross-correlation (from yellow to red: correlation coefficient (0 to 1)). In cyan: the digitized results of the current directions, which have been measured in-situ with an ADCP. The ACDP vectors are not to scale. In the background: the Gamma-MAP filtered TerraSAR-X image.

In contrast to the first ROI, where we were able to use model results for evaluation our Russian project partners have performed co-located in-situ measurements during the satellite acquisitions in this ROI. Using a research vessel and an ADCP the directions near sea surface level have been recorded. Comparing these in-situ measurements with the derived currents shows that the ACDP results near the bay are quite noisy and pointing in different directions. The derived currents are of high correlation coefficients and favor an outgoing flow as sea surface current. South of the bay, smaller but systematic errors of about 45° exist for the derived displacements of the south most linearly aligned features. There is a good overall agreement between the measured and the derived current vectors. As a quantitative evaluation, each derived vector has been compared with its 10 nearest measured neighbor vectors. Gaussian weighted by the difference, an average angular error of 57.42° with a standard deviation of 36.35° has been derived.

Although the image shows no vortical accumulations of surface film signatures, different current directions could be detected by our approach. It seems that in outgoing current is leaving the bay of Gelendzhik and mixing up with another current, which is flowing along the coastline in southeast directions. The south most line of derived currents even suggest in inflowing current component. Due to the comparably low correlation coefficient for most of these vectors, this may be neglected.

5. CONCLUSIONS

We have presented the mesoscale and sub-mesoscale derivation of se surface currents by means of tracking the signatures of biogenic sea surface films on multispectral and SAR imagery. The mesoscale results already show a promising overall quality and thus may help to refine existing models in future. The quality of the first derived measurements on sub-mesoscale sea surface currents by means of high-resolution SAR data is also highly promising.

When compared with in-situ current measurements, there are still some smaller deviations that require a further investigation. But overall, like in the mesoscale case, the existence of homogeneous flow pattern and the good correspondence to the in-situ measurements shows that we are on the right way towards the development of an robust sub-mesoscale tracking framework. For the future, we are planning to carry out more in-situ measurements and to acquire more high-resolution SAR images for the area of Gelendzhik. Due to the constraint that sea surface films need to exist (and be visible) on the imagery, we are yet restricted to certain dates, when the Russian partners are at Gelendzhik and algae blooms become evident.

The next field excursion is planned for September and October 2013. Another mentionable aspect is that we have not yet been able to acquire high-resolution SAR data of the Black Sea ROI showing signatures of eddies. But we are looking forward to the next field excursions of our Russian partners, where we have planned the next data acquisitions in conjunction with in-situ measurements.

ACKNOWLEDGMENTS

The DTeddie project is supported by the Canadian Space Agency CSA and the German Space Agency DLR by means of the announcement CSA-DLR-2010, project OCE0995. Further thanks are to Olga Lavrova and her team at the IKI (Russian Space Research Institute / Dept. of Remote Sensing) for providing the in-situ measurements and for her help by classifying the wastewater plume near the coast, which also causes a change in surface roughness, independently of the sea surface currents.

Thanks are also to the German Federal Maritime and Hydrographic Agency (BSH) for providing the electronic results of the numeric current models for the Baltic Sea under contract 2009-04.

REFERENCES

[1] Gade, M., Seppke, B., Dreschler-Fischer, L., "Mesoscale surface current fields in the Baltic Sea derived from multi-sensor satellite data", International Journal of Remote Sensing 33(10), 3122-3146 (2012).

[2] Gade, M., Alpers, M., Hühnerfuss, H., Masuko, H., Kobayashi, T., "The Imaging of Biogenic and Anthropogenic Surface Films by the Multi-frequency Multi-polarization SIR-C/X-SAR", Journal of Geophysical Research 103(C9), 18851-18866 (1998).

[3] Kahru, M., Leppänen, J.-M., Rud, O., "Cyanobacterial Blooms Cause Heating of the Sea Surface" Marine Ecology Progress 101(1-2), 1-7 (1993).

[4] Seppke, B., Dreschler-Fischer, L., Gade, M., "Towards a tracking of small scale eddies using high-resolution RADARSAT-2 and TerraSAR-X imagery", Proceedings of 1st EARSeL Workshop on Temporal Analysis of Satellite Images (2012)

[5] Lewis, J. P., "Fast Template Matching", Vision Interface '95, 15-19 (1995).

[6] Horn, B. K. P., Schunck, B. G., "Determining Optical Flow". Artificial Intelligence 17, 185-189 (1981).

[7] Seppke, B., "Untersuchungen zum Korrespondenzproblem bei der Bestimmung mesoskaliger Strömungen der Meeresoberfläche anhand von Satellitenbildern", Doctoral Thesis, University of Hamburg, Department of Informatics (2013)

[8] Mityagina, M. I., Lavrova, O. Y., Karimova, S. S., "Multi-sensor survey of seasonal variability in coastal eddy and internal wave signatures in the north-eastern Black Sea", International Journal of Remote Sensing 31(17), 4779-4790 (2010).

[9] Lucas, B. D., Kanade, T., "An Iterative Image Registration Technique with an Application to Stereo Vision", Proceedings of the 7th international joint conference on Articial intelligence (2), 674-679 (1981).

[10] Emery, W. J., Thomas, A. C., Collins, M. J., Crawford, W. R., Mackas, D. L., "An Objective Method for Computing Advective Surface Velocities from Sequential Infrared Satellite Images", Journal of Geophysical Research 91, 12865-12878 (1986).

[11] Sun, Y., "Automatic Ice Motion Retrieval from ERS-1 SAR Images Using The Optical Flow Method", International Journal of Remote Sensing 17(11), 2059-2087 (1996)

[12] Frigo, M., Johnson, S. G., "The Design and Implementation of FFTW3", Proceedings of the IEEE 93(2), 216-231 (2005).

[13] Knutsson, H., Westin, C.-F., "Normalized and Differential Convolution: Methods for Interpolation and Filtering of Incomplete and Uncertain data", Proceedings of Computer Vision and Pattern Recognition '93, 515-523 (1993)

[14] Lopes, A., Nezry, E., Touz, R., Laur, H., "Maximum a posteriori speckle filtering and first order texture models in SAR images", Geoscience and Remote Sensing Symposium IGARSS '90 Remote Sensing Science for the Nineties (10th Annual International), 2409-2412 (1990).